Optimizing Higgs factories by modifying the recoil mass *

Jiayin Gu(顾嘉荫)[1,2;1)] Ying-Ying Li(李英英)[3;2)]

[1] DESY, Notkestraße 85, D-22607 Hamburg, Germany
[2] Center for Future High Energy Physics, Institute of High Energy Physics, 19B YuquanLu, Chinese Academy of Sciences, Beijing 100049, China
[3] Department of Physics, The Hong Kong University of Science and Technology, Clear Water Bay, Kowloon, Hong Kong S.A.R., China

Abstract: It is difficult to measure the WW-fusion Higgs production process ($e^+e^- \to \nu\bar{\nu}h$) at a lepton collider with a center of mass energy of 240-250 GeV due to its small rate and the large background from the Higgsstrahlung process with an invisible Z ($e^+e^- \to hZ, Z \to \nu\bar{\nu}$). We construct a modified recoil mass variable, $m^p_{\rm recoil}$, defined using only the 3-momentum of the reconstructed Higgs particle, and show that it can separate the WW-fusion and Higgsstrahlung events better than the original recoil mass variable $m_{\rm recoil}$. Consequently, the $m^p_{\rm recoil}$ variable can be used to improve the overall precisions of the extracted Higgs couplings, in both the conventional framework and the effective-field-theory framework. We also explore the application of the $m^p_{\rm recoil}$ variable in the inclusive cross section measurements of the Higgsstrahlung process, while a quantitive analysis is left for future studies.

Keywords: CEPC, ILC, Higgs

PACS: 13.66.Fg **DOI:** 10.1088/1674-1137/42/3/033102

1 Introduction

A lepton collider running at a center of mass energy of around 240 to 250 GeV is ideal for studying the properties of the Higgs boson. It can collect a large number of Higgsstrahlung ($e^+e^- \to hZ$) events, as the Higgstrahlung process has a cross section maximized at around 250 GeV. At higher energies, the WW-fusion process of Higgs production ($e^+e^- \to \nu\bar{\nu}h$) can be measured better, as its cross section increases with energy. It is important to have good measurements of the WW-fusion process, as it provides information complementary to that from the Higgsstrahlung process. In the conventional *kappa* framework, the WW-fusion process can constrain the hWW coupling and is also an important input for the determination of the Higgs total width[3)]. In the effective-field-theory (EFT) framework, the WW-fusion and the Higgsstrahlung processes probe different combinations of EFT parameters. The inclusion of both processes, as well as the diboson one ($e^+e^- \to WW$), is crucial for discriminating different EFT parameters and obtaining robust constraints on all of them [2–5]. However, it is not guaranteed that runs at energies higher than 240–250 GeV will be available. The proposed Circular Electron Positron Collider (CEPC) in China does not currently have plans for a 350 GeV run [6]. For the Future Circular Collider (FCC)-ee at CERN [7] and the International Linear Collider (ILC) in Japan [8], a significant amount of time may also be spent on a 240 GeV/250 GeV run before moving on to higher energies. Measurements of the WW-fusion process at 240–250 GeV are therefore of great relevance to the study of Higgs physics.

It is difficult to measure the WW-fusion process at 240–250 GeV for the following two reasons. First, it has a small rate at lower energy, with a cross section of 6.72 fb at 250 GeV assuming unpolarized beams, while the total cross section of the Higgsstrahlung process is 212 fb at the same energy [6]. Second, the Higgsstrahlung process with Z decaying invisibly ($e^+e^- \to hZ, Z \to \nu\bar{\nu}$) is the dominant background for WW fusion. The two contributions to the channel $e^+e^- \to \nu\bar{\nu}h$ are shown in Fig. 1; the cross section of the former is more than six

Received 23 December 2017, Published online 6 February 2018

∗ JG is Supported by an International Postdoctoral Exchange Fellowship Program between the Office of the National Administrative Committee of Postdoctoral Researchers of China (ONACPR) and DESY. YYL is Supported by Hong Kong PhD Fellowship (HKPFS) and the Collaborative Research Fund (CRF) (HUKST4/CRF/13G)

1) E-mail: jiayin.gu@desy.de

2) E-mail: ylict@connect.ust.hk

3) See *e.g.* Ref. [1] for a recent study under this framework.

Content from this work may be used under the terms of the Creative Commons Attribution 3.0 licence. Any further distribution of this work must maintain attribution to the author(s) and the title of the work, journal citation and DOI. Article funded by SCOAP[3] and published under licence by Chinese Physical Society and the Institute of High Energy Physics of the Chinese Academy of Sciences and the Institute of Modern Physics of the Chinese Academy of Sciences and IOP Publishing Ltd

times that of the latter. With longitudinal beam polarizations, the situation is slightly better. If the signs of the polarizations are $\mathrm{sgn}(P(\mathrm{e}^-),P(\mathrm{e}^+))=(-,+)$, the WW-fusion cross section is enhanced, and by a larger factor that of $\mathrm{e}^+\mathrm{e}^-\to\mathrm{hZ}$. The recoil mass method can also be used to separate the WW-fusion and hZ events, as the reconstructed mass of the neutrino pair should center around the Z mass for hZ events. However, the discriminating power is limited by the detector resolution (especially for hadronic Higgs decays) and other effects [6, 9, 10]. A consistent treatment of the hZZ and hWW couplings is also required, since they are related by gauge invariance. In the EFT framework, the relation is complicated by the inclusion of dimension-6 operators which generate anomalous couplings with Lorentz structures different from the standard model (SM) ones.

In this paper, we try to address the issues mentioned above and further optimize the measurements in $\mathrm{e}^+\mathrm{e}^-\to\nu\bar{\nu}\mathrm{h}$ at 240–250 GeV. We first perform a collider study in Section 2, with a comparison of the recoil mass variable and its variations. We try to validate our study by closely following Ref. [10]. We point out that the variable m^p_{recoil}, defined using only the 3-momentum of the reconstructed Higgs particle, could provide a discriminating power better than the original recoil mass variable m_{recoil} does. We then implement the m_{recoil} and m^p_{recoil} distributions in the EFT global analysis in Section 3, using the framework in Ref. [3]. We point out the importance of fitting the EFT parameters directly to the binned m_{recoil} or m^p_{recoil} distribution instead of fitting them to the extracted cross sections of the WW-fusion process. We also apply m^p_{recoil} to the inclusive $\mathrm{e}^+\mathrm{e}^-\to\mathrm{hZ}$ process in Section 4 and comment on its potential use in the inclusive hZ cross section measurements. Finally, we conclude in Section 5. We provide a short summary of the EFT framework used in our analysis in Appendix A and the numerical expressions of the EFT dependence of the (modified) recoil mass distributions in Appendix B.

The following collider scenarios are considered in our study:

1) **CEPC** with $5\mathrm{ab}^{-1}$ data collected at 240 GeV, with unpolarized beams [6]. This scenario can also be thought as the earlier stage of the FCC-ee, which also plans to collect $5\mathrm{ab}^{-1}$ at 240 GeV and eventually $1.5\mathrm{ab}^{-1}$ data at 350 GeV as well [7].

2) **ILC** with $2\mathrm{ab}^{-1}$ data collected at 250 GeV and beam polarizations of $P(\mathrm{e}^-,\mathrm{e}^+)=(\pm0.8,\pm0.3)$, which could be considered as the first stage of a full program with center of mass energies up to 500 GeV [11].

For the WW-fusion measurements, we focus on the channel with the Higgs decaying to a pair of bottom quarks ($\mathrm{e}^+\mathrm{e}^-\to\nu\bar{\nu}\mathrm{h},\mathrm{h}\to\mathrm{b}\bar{\mathrm{b}}$), which has the largest branching ratio. The measurements of WW fusion at 240–250 GeV with other Higgs decay channels are not reported in the official documents due to the poor constraints (see *e.g.*, Refs. [6, 11, 12]).

2 Modified recoil mass of $\mathrm{e}^+\mathrm{e}^-\to\nu\bar{\nu}\mathrm{h}$, $\mathrm{h}\to\mathrm{b}\bar{\mathrm{b}}$

At lepton colliders, the recoil mass method can be used to reconstruct the mass of a particle without measuring its decay products. One of its most important applications is the measurement of the inclusive rate of the Higgsstrahlung process, $\mathrm{e}^+\mathrm{e}^-\to\mathrm{hZ}$. Assuming both the Higgs and Z are on mass shell, one could write the relation

$$m_h^2=E_h^2-|\vec{p}_h|^2=(\sqrt{s}-E_Z)^2-|\vec{p}_Z|^2, \tag{1}$$

where the total center of mass energy $\sqrt{s}$ is fixed up to corrections from beam energy spread and initial state radiation. By measuring the energies and momenta of the Z decay products one can reconstruct the mass of the Higgs particle. This can be used to select $\mathrm{e}^+\mathrm{e}^-\to\mathrm{hZ}$ signal events without tagging the Higgs decay products, which makes it possible to measure the inclusive cross section of this channel. It also provides the best Higgs mass measurement. For example, a precision of 5.9 MeV could be achieved with the leptonic Z decay channels of the inclusive hZ measurements at the CEPC [6].

If the Higgs decay products are measured, the recoil mass can be turned around to reconstruct the Z mass, since the following relation also holds for an $\mathrm{e}^+\mathrm{e}^-\to\mathrm{hZ}$ event,

$$m_Z^2=(\sqrt{s}-E_h)^2-|\vec{p}_h|^2=s-2\sqrt{s}E_h+m_h^2. \tag{2}$$

The recoil mass can then be defined as

$$m^2_{\mathrm{recoil}}=s-2\sqrt{s}E_h^{\mathrm{rec}}+(m_h^{\mathrm{rec}})^2, \tag{3}$$

where E_h^{rec} and m_h^{rec} are the reconstructed Higgs energy and mass. For Higgs decaying to a pair of bottom quarks, they are the total energy and the invariant mass of the two b-jets. This offers a way to separate the Higgsstrahlung events with an invisible Z ($\mathrm{e}^+\mathrm{e}^-\to\mathrm{hZ},\mathrm{Z}\to\nu\bar{\nu}$) from the WW-fusion events, both contributing to the channel $\mathrm{e}^+\mathrm{e}^-\to\nu\bar{\nu}\mathrm{h}$, as shown in Fig. 1. However, due to finite jet resolutions, beam energy spread and other effects, the recoil mass distribution of the hZ events has a rather large spread. This limits it discriminating power, especially at the energy 240–250 GeV, for which the recoil mass distribution of the WW-fusion events spreads around the same region. We also find that for Higgs decaying to a pair of b-jets ($\mathrm{h}\to\mathrm{b}\bar{\mathrm{b}}$) the uncertainty on the recoil mass is dominated by the energy and momentum resolutions of the b-jets. This is also obvious from the observation that the recoil mass distribution for the Higgs mass reconstruction in Eq. (1) is much narrower for the leptonic Z decay channel than for the hadronic one (see *e.g.* Ref. [6]).

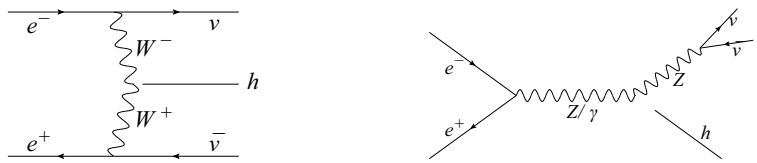

Fig. 1. The two processes that contributes to the $e^+e^- \to \nu\bar{\nu}h$ channel. (a) The WW-fusion process of Higgs production. (b) The Higgsstrahlung process with Z decaying to a pair of neutrinos.

While the recoil mass defined in Eq. (3) makes use of all the kinematic information, it does not make any assumption on the value of the Higgs mass. Both the Higgs width and the projected uncertainty of its mass are at the MeV level and can be neglected compared with the effects of jet resolution. Using the information of the Higgs mass, two modifications of the recoil mass can be constructed. The first, using only the reconstructed Higgs energy as the measurement input, is defined as

$$(m^E_{\rm recoil})^2 = s - 2\sqrt{s}E^{\rm rec}_h + m^2_h, \tag{4}$$

where m_h is fixed to be the Higgs mass, 125.09 GeV. The other, using only the reconstructed 3-momentum ($\vec{p}^{\rm rec}_h$) of the Higgs, is defined as

$$(m^p_{\rm recoil})^2 = s - 2\sqrt{s}\sqrt{m^2_h + |\vec{p}^{\rm rec}_h|^2} + m^2_h, \tag{5}$$

where m_h is again fixed to be 125.09 GeV. At the truth level, $m_{\rm recoil}$, $m^E_{\rm recoil}$ and $m^p_{\rm recoil}$ are all equivalent. However, the uncertainties in the energy and momentum measurements certainty have different impacts on the three variables. To illustrate this impact, we define, for a given event, a set of five parameters $\{\delta_m, \delta^E_m, \delta^p_m, \delta_E, \delta_p\}$ which parameterize the differences between the reconstructed quantities and the true ones, with

$$m_{\rm recoil} = m^{\rm true}_{\rm recoil}(1+\delta_m), \quad m^E_{\rm recoil} = m^{\rm true}_{\rm recoil}(1+\delta^E_m), \quad m^p_{\rm recoil} = m^{\rm true}_{\rm recoil}(1+\delta^p_m), \tag{6}$$

and

$$E^{\rm rec}_h = E_h(1+\delta_E), \qquad |\vec{p}^{\rm rec}_h| = |\vec{p}_h|(1+\delta_p), \tag{7}$$

where $m^{\rm true}_{\rm recoil}$ is the true parton level recoil mass, and E_h and $\vec{p}_h$ are the true energy and 3-momentum of the Higgs respectively. For hZ events, $m^{\rm true}_{\rm recoil} = m_Z$ (assuming it is on shell), and the three parameters δ_m, δ^E_m and δ^p_m can be written in terms of δ_E and δ_p. At leading order, they are given (for hZ events) by

$$\begin{aligned}
\delta_m &\approx -\frac{1}{m^2_Z}\left[(\sqrt{s}-E_h)E_h\delta_E + |\vec{p}_h|^2\delta_p\right],\\
\delta^E_m &\approx -\frac{\sqrt{s}}{m^2_Z}E_h\delta_E,\\
\delta^p_m &\approx -\frac{\sqrt{s}}{m^2_Z}\frac{|\vec{p}_h|^2}{E_h}\delta_p.
\end{aligned} \tag{8}$$

Note that δ_E and δ_p can be either positive or negative. The overall negative coefficients in Eq. (8) indicates that if the measured energy or 3-momentum of the Higgs is larger than its actual value, the recoil mass variables will be smaller than the Z mass, and *vice versa*. For a fixed center of mass energy ($\sqrt{s}$=240 GeV or 250 GeV), the values of E_h and $|\vec{p}_h|$ are fixed. In particular, near the hZ threshold $|\vec{p}_h|$ is significantly smaller than E_h. With $|\vec{p}_h| \approx 51$ GeV and $E_h \approx 135$ GeV at $\sqrt{s}=240$ GeV, and $|\vec{p}_h| \approx 62$ GeV and $E_h \approx 140$ GeV at $\sqrt{s}=250$ GeV, Eq. (8) thus becomes

$$\delta_m \;/\; \delta^E_m \;/\; \delta^p_m \approx \begin{cases} -1.7\delta_E - 0.32\delta_p \;/\; -3.9\delta_E \;/\; -0.57\delta_p & \text{at 240GeV} \\ -1.9\delta_E - 0.46\delta_p \;/\; -4.2\delta_E \;/\; -0.83\delta_p & \text{at 250GeV} \end{cases}, \tag{9}$$

where the small coefficients of δ_p come from a suppression factor of $\sim |\vec{p}_h|^2/E^2_h$ relative to those of δ_E, shown in Eq. (8). The distributions of δ_E and δ_p for $e^+e^- \to hZ, Z \to \nu\bar{\nu}, h \to b\bar{b}$ at CEPC 240 GeV are shown in Fig. 2(a), after applying the selection cuts, which include a Higgs-mass-window cut of $105\,{\rm GeV} < m^{\rm rec}_h < 135\,{\rm GeV}$ on the b-jet pair.

While δ_p has a slightly larger spread than δ_E, its coefficients in Eq. (9) are much smaller. We therefore expect the distribution $m^p_{\rm recoil}$ to have the smallest spread, and that of $m^E_{\rm recoil}$ to have the largest. This is verified in Fig. 2(b), where the distributions of $m_{\rm recoil}$, $m^E_{\rm recoil}$ and $m^p_{\rm recoil}$ are shown. For the WW-fusion events, we expect a less significant difference among the distributions of the three variables (which are shown later in Figs. 3 & 4), since they do not have a Z in the event. The corresponding distributions for ILC 250 GeV are very similar to the ones in Fig. 2.

The distribution of δ_E in Fig. 2 is asymmetric, suggesting that on average the measured energy of the b-jet pair is smaller than its actual value. This is due to the fact that in our simulation we do not apply any jet

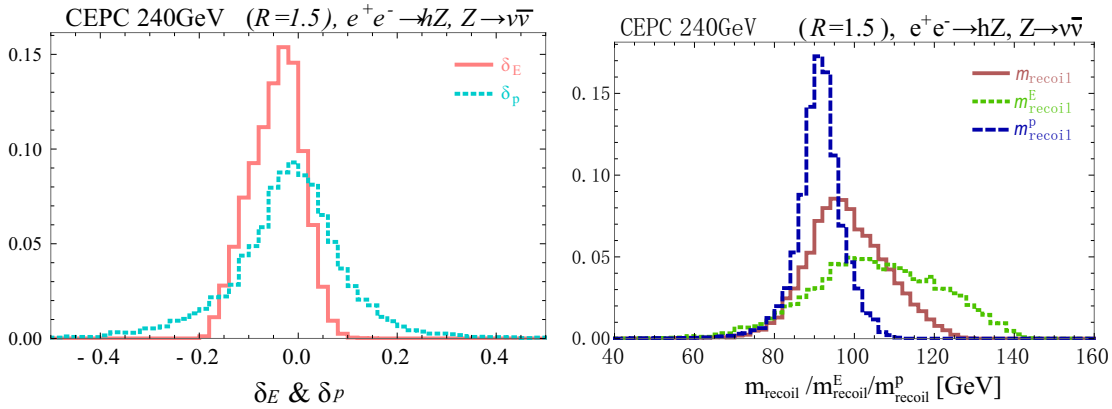

Fig. 2. (color online) (a) The distributions of δ_E and δ_p (defined in Eq. (7)) for $e^+e^- \to hZ, Z\to\nu\bar{\nu}, h\to b\bar{b}$ at CEPC 240 GeV, after applying a Higgs-mass-window cut of $105\,\text{GeV} < m_h^{\text{rec}} < 135\,\text{GeV}$. (b) The corresponding distributions of m_{recoil}, m^E_{recoil} and m^p_{recoil}, defined in Eqs. (3)–(5). A radius of $R=1.5$ is used in the jet clustering algorithm. The details of the simulations and selection cuts are stated later in this section.

energy corrections, which are widely used in the LHC experiments [13, 14]. As a result, the central values of the m_{recoil} and m^E_{recoil} distributions are also shifted to be larger than m_Z. Assuming a jet energy correction mechanism will be implemented in the future lepton collider(s), one would expect a corrected central value and also some improvements in the energy measurement, and the m_{recoil} (and m^E_{recoil}) distribution will have a peak value around m_Z and a slightly smaller spread. We do not expect the lack of jet energy correction to have a significant impact on our results, since the m^p_{recoil} distribution still has a much smaller spread, due to the parametric suppression of its uncertainty near the hZ threshold as discussed above[1)].

Having found that the variable m^p_{recoil} could reconstruct the Z mass better than m_{recoil}, we perform an analysis based on a fast simulation to explicitly examine their discriminating powers for WW-fusion and hZ events at the CEPC 240 GeV (with unpolarized beams) and ILC 250 GeV (assuming $P(e^-,e^+)=(-0.8,+0.3)$). We generated events for both processes using `Madgraph5` [15], which were showered with `Pythia` [16] before passing to `Delphes` [17] with ILD cards (using the detector geometry and flavor tagging efficiencies given in Ref. [18]) for detector simulations. The interference terms between the WW-fusion and hZ processes are ignored. The effects of ISR photons are not considered in the simulation with `Madgraph5`. However, we expect their effects to be much smaller than that of jet resolution[2)]. We use the ILC analysis in Ref. [10] as a guide to validate our results from the simple simulation. While the Durham jet clustering algorithm was used in Ref. [10], it was pointed out that the anti-k_t jet algorithm with jet radius $R=1.5$ has a similar performance in the Higgs invariant mass reconstruction, which is used in our simulation. We also follow closely the selection cuts in Ref. [10]. In particular, each event is required to have exactly two b-jets and a cut on the invariant mass of the b-jet pair, $105\,\text{GeV} < m_h^{\text{rec}} < 135\,\text{GeV}$, is applied to reduce the backgrounds. The cuts related to variables in the Durham jet clustering algorithm are replaced by the simple requirement on jet number (=2) in each event. After event selections, we scale the number of signal events of ILC 250 GeV to those in Ref. [10] (normalized to 2ab^{-1}). A similar scaling is also applied for CEPC, taking account of the differences in cross sections and selection efficiencies between CEPC and ILC.

The composition of the background in the $e^+e^- \to \nu\bar{\nu}h$ channel is also listed in Ref. [10]. The major components are $\nu\bar{\nu}b\bar{b}$ and $q\bar{q}$, which contribute to 42% and 34% respectively of the total background after selection cuts. The $q\bar{q}$ background is difficult to simulate due to its huge cross section and tiny selection efficiency. For simplicity, we simulate only the $\nu\bar{\nu}b\bar{b}$ background, apply the selection cuts and scale it up to match the total background number, given in Ref. [10] and normalized to our run scenarios. We expect this simple treatment to provide a reasonable estimation of the effects of the backgrounds.

After selection cuts, the m_{recoil} and m^p_{recoil} distributions of hZ ($Z\to\nu\bar{\nu}$), WW-fusion and background events are shown in Fig. 3 for ILC 250 GeV (2ab^{-1} data with $P(e^-,e^+)=(-0.8,+0.3)$) and Fig. 4 for CEPC 240 GeV (5ab^{-1} data, unpolarized beams). In Figs. 3 and 4, the m_{recoil} (m^p_{recoil}) distribution is shown on the left (right), while the distributions in the bottom panels are simply magnified versions of those in the top panels.

1) We thank Zhen Liu for very valuable discussions on the topic of jet energy corrections.

2) See Ref. [19] for a thorough discussion on the ISR effects of Higgs production at lepton colliders.

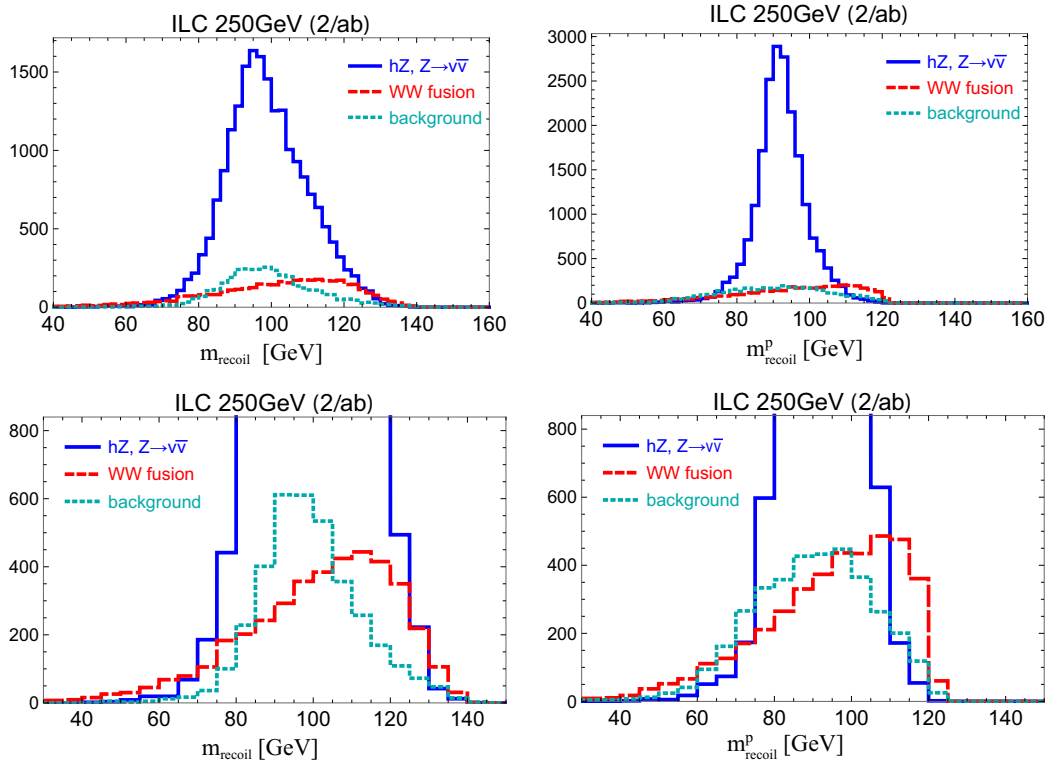

Fig. 3. (color online) The $m_{\rm recoil}$ (left) and $m^p_{\rm recoil}$ (right) distributions of hZ ($Z \to \nu\bar{\nu}$), WW-fusion and background events after selection cuts for ILC 250 GeV with a luminosity of $2{\rm ab}^{-1}$ and beam polarization $P(e^-,e^+)=(-0.8,+0.3)$. The distributions in the bottom panels are magnified versions of the ones in the top panels (and also have a different bin size).

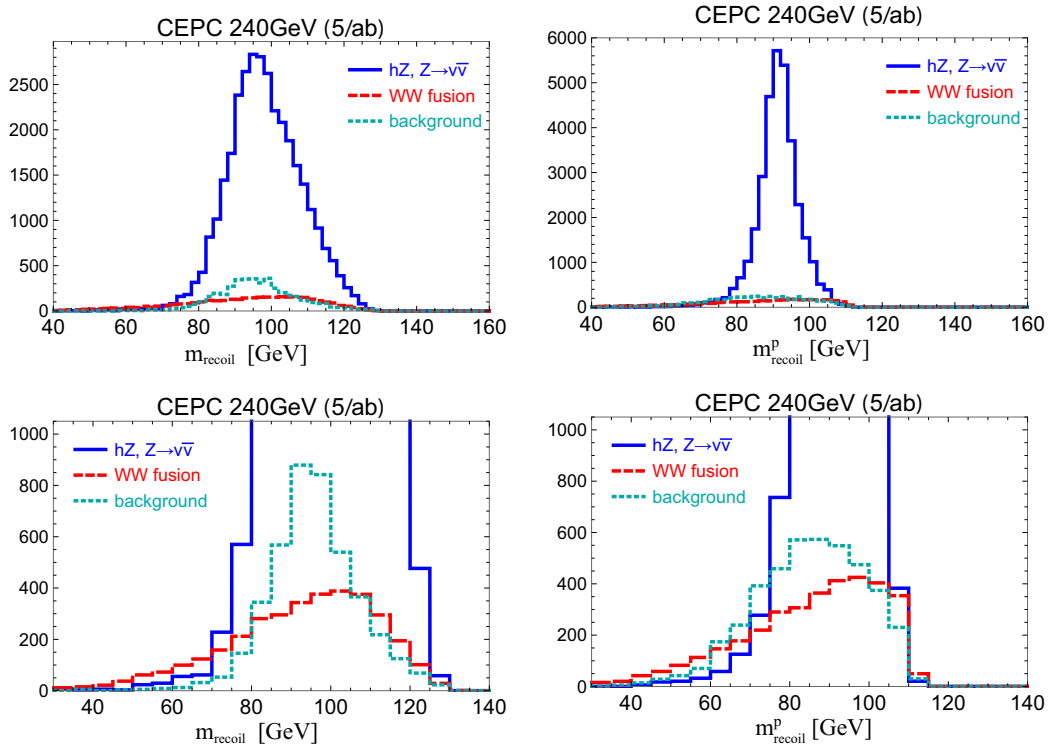

Fig. 4. (color online) The $m_{\rm recoil}$ (left) and $m^p_{\rm recoil}$ (right) distributions of hZ ($Z\to\nu\bar{\nu}$), WW-fusion and background events after selection cuts for CEPC 240 GeV with $5{\rm ab}^{-1}$ data and unpolarized beams. The distributions in the bottom panels are magnified versions of the ones in the top panels (and also have a different bin size).

To check the validity of our results, we compared our $m_{\rm recoil}$ distributions those in Refs. [6, 10] and found a reasonable agreement in terms of spread ranges and distribution shapes. Comparing the $m_{\rm recoil}$ and $m^p_{\rm recoil}$ distributions in Figs. 3 and 4, it is clear that $m^p_{\rm recoil}$ provides a better discrimination between hZ and WW-fusion events, with the $m^p_{\rm recoil}$ distribution of hZ having a much sharper peak around the Z mass than the $m_{\rm recoil}$ one. On the other hand, the $m^p_{\rm recoil}$ distribution of the $\nu\bar{\nu}b\bar{b}$ background has a more even spread than the $m_{\rm recoil}$ one. This is because for the $\nu\bar{\nu}b\bar{b}$ background, the $b\bar{b}$ pair does not come from the Higgs decay. Using the wrong mass assumption therefore makes the reconstruction of Z mass worse.

Following Ref. [10], we apply a χ^2 fit to the binned $m_{\rm recoil}$ and $m^p_{\rm recoil}$ distributions to extract the precisions (one-sigma uncertainties) of the hZ and WW cross sections, denoted as $\sigma_{\rm hZ}$ and $\sigma_{\rm WW\to h}$. This is done by treating the overall rates, $\sigma_{\rm hZ}$ and $\sigma_{\rm WW\to h}$ as free parameters while assuming perfect knowledge of the shapes of the distributions. Reference [10] also treats the overall cross section of the background ($\sigma_{\rm bg}$) as a free parameter. We consider two cases with $\sigma_{\rm bg}$ treated as a free parameter as well as fixing it to the predicted value. The total χ^2 of the $m_{\rm recoil}$ or $m^p_{\rm recoil}$ distribution is given by

$$\chi^2=\sum_i \frac{(n^i_{\rm theory}-n^i_{\rm exp})^2}{n^i_{\rm exp}}, \tag{10}$$

where for each bin i, $n^i_{\rm exp}$ is the expected number of events from simulation and $n^i_{\rm theory}$ is a function of $\sigma_{\rm hZ}$ and $\sigma_{\rm WW\to h}$ (and $\sigma_{\rm bg}$). To ensure enough statistics in each bin, we choose a bin size of 5 GeV, except for the first and last bin, which are chosen to include all the events below 65 GeV (60 GeV) and above 130 GeV (115 GeV) for the $m_{\rm recoil}$ ($m^p_{\rm recoil}$) distribution at ILC, and all the events below 65 GeV (60 GeV) and above 120 GeV (110 GeV) for the $m_{\rm recoil}$ ($m^p_{\rm recoil}$) distribution at CEPC. The results of the χ^2 fits are presented in Table 1 for ILC 250 GeV (2ab^{-1} data with $P(\mathrm{e}^-,\mathrm{e}^+)=(-0.8,+0.3)$) and Table 2 for CEPC 240 GeV (5ab^{-1} data, unpolarized beams).

Overall, our results on the precision of the WW-fusion cross section are slightly worse than those in Ref. [10] (if normalized to the same luminosity) and the CEPC preCDR [6]. This is not surprising, since the results could depend on details of the simulation, for which we only performed a simplified study. In what follows, we shall focus on the relative difference between the results from $m_{\rm recoil}$ and $m^p_{\rm recoil}$. While the distributions of $m^p_{\rm recoil}$ clearly better separate the hZ and WW-fusion events, as shown in Figs. 3 and 4, in the 3-parameter fit (shown on the left panels of Tables 1 and 2) the precision of $\sigma_{\rm WW\to h}$ from the $m^p_{\rm recoil}$ distribution is similar to (or even worse than) that of $m_{\rm recoil}$, due to the fact that WW-fusion and background events have a larger overlap in the $m^p_{\rm recoil}$ distribution than in the $m_{\rm recoil}$ one. $m^p_{\rm recoil}$ nevertheless significantly improves the precisions of $\sigma_{\rm hZ}$ and $\sigma_{\rm bg}$ in the 3-parameter fit. Assuming a good knowledge of the background, one may also fix the background cross section to the predicted value. In the 2-parameter fit with $\sigma_{\rm hZ}$ and $\sigma_{\rm WW\to h}$, the $m^p_{\rm recoil}$ distribution indeed provides a significantly better constraint on $\sigma_{\rm WW\to h}$, with an improvement of about 30% at ILC and 20% at CEPC, compared with the constraint from the $m_{\rm recoil}$ distribution.

While the cross section $\sigma(\mathrm{hZ},\mathrm{h}\to \mathrm{b}\bar{\mathrm{b}},\mathrm{Z}\to\nu\bar{\nu})$ is treated as a free parameter in the fit, it can be constrained by the measurements of hZ using visible Z decays, assuming the Z branching ratios are well known. A combined χ^2 fit, also including measurements of $\sigma(\mathrm{hZ},\mathrm{h}\to\mathrm{b}\bar{\mathrm{b}},\mathrm{Z}\to\mathrm{ll/qq})$, has been performed in a recent ILC analysis [20][1)]. In a global analysis of Higgs couplings, one could also directly use the results in Table 1 and 2 and the measurements of $\sigma(\mathrm{hZ},\mathrm{h}\to\mathrm{b}\bar{\mathrm{b}},\mathrm{Z}\to\mathrm{ll/qq})$ as inputs without taking an extra step to combine them first. However, as we point out later, it is important to take account of the correlation between $\sigma_{\rm hZ}$ and $\sigma_{\rm WW\to h}$ in such global analyses.

In the *kappa* framework with the hZZ and hWW couplings treated as independent parameters, the WW-fusion measurement is an important input for constraining the hWW coupling (with the other being the Higgs decay, $\mathrm{h}\to\mathrm{WW}^*$). With a 20%–30% improvement on the precision of the WW-fusion cross section, a sizable improvement for the constraint on the hWW coupling is expected. The WW-fusion cross section is also an important input for the determination of the Higgs total width, following the relation [6][2)]

$$\Gamma_h\propto\frac{\Gamma(\mathrm{h}\to\mathrm{b}\bar{\mathrm{b}})}{\mathrm{BR}(\mathrm{h}\to\mathrm{b}\bar{\mathrm{b}})}\propto\frac{\sigma(\nu\bar{\nu}\mathrm{h},\mathrm{h}\to\mathrm{b}\bar{\mathrm{b}})}{\mathrm{BR}(\mathrm{h}\to\mathrm{b}\bar{\mathrm{b}})\cdot\mathrm{BR}(\mathrm{h}\to\mathrm{WW}^*)}, \tag{11}$$

where, following the usual convention, $\sigma(\nu\bar{\nu}\mathrm{h})$ denotes only the WW-fusion contribution to it. With a 20%–30% improvement on the precision of $\sigma(\nu\bar{\nu}\mathrm{h},\mathrm{h}\to\mathrm{b}\bar{\mathrm{b}})$, as well as some possible improvement on the determination of $\mathrm{BR}(\mathrm{h}\to\mathrm{b}\bar{\mathrm{b}})$ from a better measurement of $\sigma(\mathrm{hZ},\mathrm{Z}\to\nu\bar{\nu},\mathrm{h}\to\mathrm{b}\bar{\mathrm{b}})$, the precision of the Higgs total width obtained using Eq. (11) could be improved by at least 20%–30% using the $m^p_{\rm recoil}$ variable.

1) We thank Junping Tian for pointing out this analysis to us.

2) It should be noted that, despite the usual claim of being model independent, Eq. (11) explicitly assumes that the hWW coupling is independent of the energy scale (*i.e.*, anomalous couplings such as $\mathrm{hW}^{\mu\nu}\mathrm{W}_{\mu\nu}$ are absent), which is not true under the more general EFT framework.

Table 1. The one sigma uncertainties and correlations of the cross sections of the Higgsstrahlung process with an invisible Z ($\sigma_{\rm hZ}$) and the WW-fusion process ($\sigma_{\rm WW\to h}$) at ILC 250 GeV from a fit to the $m_{\rm recoil}$ (top panel) and $m^p_{\rm recoil}$ (bottom panel) distributions. A total luminosity of $2{\rm ab}^{-1}$ with beam polarization of $P({\rm e}^-,{\rm e}^+)=(-0.8,+0.3)$ is assumed. In the 3-parameter fit on the left panel, the overall normalization of the background is treated as a free parameter in the fit. In the 2-parameter fit on the left panel, the total number of background events is fixed to the predicted value.

ILC 250 GeV, $2{\rm ab}^{-1}$, uncertainties normalized to SM predictions							
$m_{\rm recoil}$	3-parameter fit				fixing $\sigma_{\rm bg}$		
	uncertainty	correlation matrix			uncertainty	correlation matrix	
		$\sigma_{\rm hZ}$	$\sigma_{\rm WW\to h}$	$\sigma_{\rm bg}$		$\sigma_{\rm hZ}$	$\sigma_{\rm WW\to h}$
$\sigma_{\rm hZ}$	0.049	1	0.47	−0.97	0.011	1	−0.69
$\sigma_{\rm WW\to h}$	0.063		1	−0.63	0.045		1
$\sigma_{\rm bg}$	0.31			1			
$m^p_{\rm recoil}$	3-parameter fit				fixing $\sigma_{\rm bg}$		
	uncertainty	correlation matrix			uncertainty	correlation matrix	
		$\sigma_{\rm hZ}$	$\sigma_{\rm WW\to h}$	$\sigma_{\rm bg}$		$\sigma_{\rm hZ}$	$\sigma_{\rm WW\to h}$
$\sigma_{\rm hZ}$	0.010	1	0.21	−0.51	0.0088	1	−0.46
$\sigma_{\rm WW\to h}$	0.059		1	−0.83	0.033		1
$\sigma_{\rm bg}$	0.088			1			

Table 2. The one sigma uncertainties and correlations of the cross sections of the Higgsstrahlung process with an invisible Z ($\sigma_{\rm hZ}$) and the WW-fusion process ($\sigma_{\rm WW\to h}$) at CEPC 240 GeV from a fit to the $m_{\rm recoil}$ (top panel) and $m^p_{\rm recoil}$ (bottom panel) distributions. A total luminosity of $5{\rm ab}^{-1}$ with unpolarized beams is assumed. In the 3-parameter fit on the left panel, the overall normalization of the background is treated as a free parameter in the fit. In the 2-parameter fit on the left panel, the total number of background events is fixed to the predicted value.

CEPC 240 GeV, $5{\rm ab}^{-1}$, uncertainties normalized to SM predictions							
$m_{\rm recoil}$	3-parameter fit				fixing $\sigma_{\rm bg}$		
	uncertainty	correlation matrix			uncertainty	correlation matrix	
		$\sigma_{\rm hZ}$	$\sigma_{\rm WW\to h}$	$\sigma_{\rm bg}$		$\sigma_{\rm hZ}$	$\sigma_{\rm WW\to h}$
$\sigma_{\rm hZ}$	0.024	1	0.28	−0.95	0.0077	1	−0.61
$\sigma_{\rm WW\to h}$	0.058		1	−0.47	0.051		1
$\sigma_{\rm bg}$	0.20			1			
$m^p_{\rm recoil}$	3-parameter fit				fixing $\sigma_{\rm bg}$		
	uncertainty	correlation matrix			uncertainty	correlation matrix	
		$\sigma_{\rm hZ}$	$\sigma_{\rm WW\to h}$	$\sigma_{\rm bg}$		$\sigma_{\rm hZ}$	$\sigma_{\rm WW\to h}$
$\sigma_{\rm hZ}$	0.0071	1	0.098	−0.35	0.0066	1	−0.45
$\sigma_{\rm WW\to h}$	0.083		1	−0.87	0.041		1
$\sigma_{\rm bg}$	0.082			1			

To conclude this section, we would like to emphasize that, while we try our best to validate our results, they do rely on simple simulations and should be explicitly tested by experimental groups with proper simulation tools. The fits performed in obtaining the results in Tables 1 and 2 also assume a perfect knowledge of the distribution shapes for each process, which may not be a good assumption in an actual experiment. We also include only the $\nu\bar{\nu}b\bar{b}$ background, while other backgrounds may have different kinematic features. Nevertheless, we expect our results to still hold qualitatively due to the simple reasoning that $m^p_{\rm recoil}$ has a smaller uncertainty and better reconstructs the Z mass.

3 Improving Higgs coupling constraints in the EFT framework

Having explored the capability of the $m^p_{\rm recoil}$ variable in improving the measurement of the WW-fusion process, we are now ready to examine its impact on the determination of the Higgs couplings. We choose to study the Higgs coupling constraints in a global effective-field-theory (EFT) framework with dimension-six (D6) operators[1)]. Such a framework has several advantages. First, assuming the scale of new physics is high, EFT with D6 operators gives a good parameterization of the effects of new physics and the results can be mapped to

1) For recent Higgs EFT studies in the contexts of future lepton colliders, see Refs. [2–5, 21–29].

any specific model that satisfies the assumptions of the framework. Second, it takes account of the connections among different measurements. For instance, some operators contribute to both Higgs processes and the dibson process, and the triple gauge coupling (TGC) measurements from the diboson process can thus help the overall constraints on the Higgs couplings [30]. Gauge invariance is also imposed by construction in the EFT framework. We focus on the CEPC 240 GeV and follow Ref. [3] in terms of the basis choice and measurement inputs. In particular, focusing on the Higgs and diboson measurements at 240 GeV, and making reasonable assumptions, a total of 11 parameters are sufficient to describe the contributions from the D6 operators. A short summary of the framework in Ref. [3] is provided in Appendix . The methods we propose should nevertheless be applicable to other collider scenarios and frameworks.

A few important differences between the cross-section fit in Section 2 and the EFT analysis should be noted. While not specifically mentioned, the cross-section fit does make assumptions on the new physics, in particular that it only modifies the overall rates, not the differential distributions, of the hZ and WW-fusion processes. In the cross-section fit, the hWW and hZZ couplings are also assumed to be independent, regardless of their relation from gauge invariance. The EFT analysis, while imposing gauge invariance, contains anomalous couplings of the form $\mathrm{hZ}_{\mu\nu}\mathrm{Z}^{\mu\nu}$ and $\mathrm{hZ}_{\mu}\partial_{\nu}\mathrm{Z}^{\mu\nu}$ (and the same for W) which have different momentum dependences from the SM couplings due to the extra derivatives. The potential new physics contribution to the $\mathrm{hZ}\gamma$ vertex is also included in the EFT analysis, which could contribute to $\mathrm{e^+e^-}\to\mathrm{hZ}$ via an s-channel photon. It is thus better to directly fit the EFT parameters to the m_{recoil} or m^p_{recoil} distribution of the inclusive $\mathrm{e^+e^-}\to\nu\bar{\nu}\mathrm{h}$ process instead of fitting them to the extracted precisions of cross sections from Section 2. By fitting to the inclusive $\mathrm{e^+e^-}\to\nu\bar{\nu}\mathrm{h}$ process we also include the interference term of WW-fusion and hZ processes, which is usually ignored in cross-section fits. The expressions for the total cross section of $\mathrm{e^+e^-}\to\nu\bar{\nu}\mathrm{h}$ and the (binned) differential ones of the m_{recoil} and m^p_{recoil} distributions in terms of the EFT parameters are listed in Appendix B.

The measurement inputs of the Higgsstrahlung ($\mathrm{e^+e^-}\to\mathrm{hZ}$) and diboson ($\mathrm{e^+e^-}\to\mathrm{WW}$) processes at CEPC 240 GeV are listed in Table 3. The estimations of hZ measurements are taken from Ref. [31], which updates the ones in the CEPC preCDR [6]. In addition, the angular observables of $\mathrm{e^+e^-}\to\mathrm{hZ}$ in Ref. [22] are included, for which we use only the channel $\mathrm{e^+e^-}\to\mathrm{hZ},\mathrm{h}\to\mathrm{b\bar{b}},\mathrm{Z}\to\mathrm{l^+l^-}$ and assume a fixed 60% signal selection efficiency, following Refs. [3, 24]. For the TGC measurements, we follow the treatment in Ref. [3], which adopts the one in Ref. [32] with the addition of a universal 1% systematic uncertainty in each bin of all differential distributions. We directly list the resultant one-sigma constraints of the anomalous TGC parameters and their correlations in Table 3. We construct the total χ^2 by summing over the χ^2s of all measurements and perform global fits to obtain the precision reaches (one-sigma bounds) of the relevant EFT parameters.

We consider three scenarios in the global analysis. All three use the inputs on Higgsstrahlung and TGC measurements in Table 2, but different information on the measurement of $\mathrm{e^+e^-}\to\nu\bar{\nu}\mathrm{h}$. The first one uses only the total rate of $\mathrm{e^+e^-}\to\nu\bar{\nu}\mathrm{h}$. The second and third use the information in the m_{recoil} and m^p_{recoil} distributions respectively, with the EFT parameters directly fitted to

Table 3. A summary of the measurement inputs from $\mathrm{e^+e^-}\to\mathrm{hZ}$ and $\mathrm{e^+e^-}\to\mathrm{WW}$ at CEPC 240 GeV used in the EFT fit, assuming a total luminosity of $5\mathrm{ab}^{-1}$ and unpolarized beams. Inputs on rate measurements of $\mathrm{e^+e^-}\to\mathrm{hZ}$ are from Ref. [31], which updates the estimations in the preCDR [6]. For the precision of $\sigma(\mathrm{hZ})\times\mathrm{BR}(\mathrm{h}\to\mathrm{b\bar{b}})$ (marked by a star ★), we have excluded the contribution from $\mathrm{e^+e^-}\to\mathrm{hZ},\mathrm{Z}\to\nu\bar{\nu},\mathrm{h}\to\mathrm{b\bar{b}}$ to avoid double counting with $\mathrm{e^+e^-}\to\nu\bar{\nu}\mathrm{h},\mathrm{h}\to\mathrm{b\bar{b}}$. The angular observables in $\mathrm{e^+e^-}\to\mathrm{hZ},\mathrm{h}\to\mathrm{b\bar{b}},\mathrm{Z}\to\mathrm{l^+l^-}$ are included, assuming a 60% signal selection efficiency. The constraints on aTGC parameters from measurements of $\mathrm{e^+e^-}\to\mathrm{WW}$ are obtained following the treatments in Ref. [3].

CEPC 240 GeV, $5\mathrm{ab}^{-1}$, unpolarized beams						
$\mathrm{e^+e^-}\to\mathrm{hZ}$		$\mathrm{e^+e^-}\to\mathrm{WW}$				
$\sigma(\mathrm{e^+e^-}\to\mathrm{hZ})$	0.50%	uncertainty		correlation matrix		
	$\sigma(\mathrm{hZ})\times\mathrm{BR}$			$\delta g_{1,\mathrm{Z}}$	$\delta\kappa_\gamma$	λ_Z
$\mathrm{h}\to\mathrm{b\bar{b}}$	0.24%★	$\delta g_{1,Z}$	6.4×10^{-3}	1	0.068	-0.93
$\mathrm{h}\to\mathrm{c\bar{c}}$	2.5%	$\delta\kappa_\gamma$	3.5×10^{-3}		1	-0.40
$\mathrm{h}\to\mathrm{gg}$	1.2%	λ_Z	6.3×10^{-3}			1
$\mathrm{h}\to\tau\tau$	1.0%					
$\mathrm{h}\to\mathrm{WW}^*$	1.0%					
$\mathrm{h}\to\mathrm{ZZ}^*$	4.3%	angular observables in				
$\mathrm{h}\to\gamma\gamma$	9.0%	$\mathrm{e^+e^-}\to\mathrm{hZ},\mathrm{h}\to\mathrm{b\bar{b}},\mathrm{Z}\to\mathrm{l^+l^-}$				
$\mathrm{h}\to\mu\mu$	12%	are also included.				
$\mathrm{h}\to\mathrm{Z}\gamma$	25%					

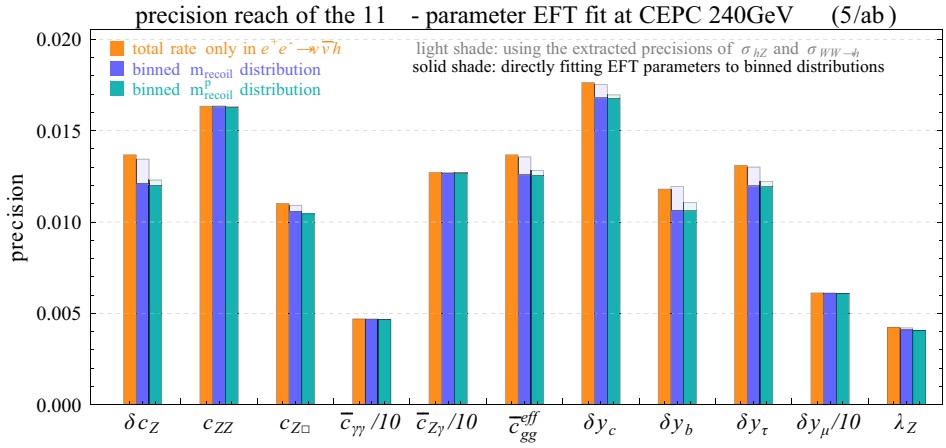

Fig. 5. (color online) The one-sigma precision reach of the 11-parameter fit in the EFT framework at CEPC 240 GeV with 5ab^{-1} data and unpolarized beams. See Appendix for the definitions of parameters. Three scenarios are shown, which differ in the information used for the $e^+e^- \to \nu\bar{\nu}h$ measurement. The first uses only the total rate of $e^+e^- \to \nu\bar{\nu}h$. The second and third use the $m_{\rm recoil}$ and $m^p_{\rm recoil}$ distributions respectively, and contain two sub-scenarios. The one shown by the light shaded columns uses the extracted precisions of σ_{hZ} and $\sigma_{WW\to h}$ in Section 2 (the two-parameter fit in the right-hand panel of Table 2, correlation ignored). The one shown by the solid columns is obtained from a direct fit to the binned $m_{\rm recoil}$ ($m^p_{\rm recoil}$) distribution.

the binned distributions. We also compare the reach with the more conventional method of fitting the EFT parameters to the extracted precisions of hZ and WW-fusion cross sections in Table 2, ignoring the correlation between the two cross sections (which is often not reported). Since the background is assumed to be SM-like in the EFT analysis[1)], for the extracted precision of cross sections we also use the results of the two-parameter fit with fixed background, shown in the right-hand panel of Table 2. The results of the 11-parameter fit are presented in Fig. 5.

Comparing the reaches of the three scenarios (shown by the orange, blue and cyan columns in Fig. 5), we indeed observe a non-negligible improvement in the overall reach if the information in the $m_{\rm recoil}$ or $m^p_{\rm recoil}$ distribution is used. In particular, the reach on the parameter δc_Z (corresponding to a shift in the SM hZZ and hWW couplings) is improved by more than 10%. Consequently, the reach on $\bar{c}^{\rm eff}_{gg}$, δy_c, δy_b and δy_τ, which contribute to the Higgs decay to gg, $c\bar{c}$, $b\bar{b}$ and $\tau\bar{\tau}$, have also been improved by a similar (or slightly less) factor. The reach with the $m^p_{\rm recoil}$ distribution is better than that with $m_{\rm recoil}$, as we expected. However, the relative improvement from $m_{\rm recoil}$ to $m^p_{\rm recoil}$ turns out to be very marginal. We also find that, if fitting the EFT parameters to the extracted cross sections σ_{hZ} and $\sigma_{WW\to h}$ without taking count of their correlation (the results are shown with light shades for the 2nd and 3rd columns), the reaches are worse than those from directly fitting the EFT parameters to the distributions, in particular for the $m_{\rm recoil}$ distribution. This is because, as shown in Section 2, the uncertainties of σ_{hZ} and $\sigma_{WW\to h}$ have a large correlation between them due to the difficulty in separating the two, in particular for the $m_{\rm recoil}$ distribution. This correlation is not usually reported in official documents, and its omission could lead to a considerable impact on the overall reach. It should be noted that our results using only the total rate of $e^+e^- \to \nu\bar{\nu}h$ are worse than the corresponding ones in Ref. [3]. This is because our estimation of the rate measurement of $e^+e^- \to \nu\bar{\nu}h$ is more conservative than the one in Ref. [3], which is derived from the CEPC preCDR [6]. If the overall cross section measurement of $e^+e^- \to \nu\bar{\nu}h$ can be improved (*e.g.* by optimizing the selection cuts), we expect the use of $m_{\rm recoil}$ and $m^p_{\rm recoil}$ distributions would also bring a more significant improvement on the overall reach of the EFT fit. We have also chosen very conservative bin sizes to control the uncertainties in each bin from simulation. Further optimizations of the analysis may also provide substantial improvements on the reach with the $m_{\rm recoil}$ and $m^p_{\rm recoil}$ distributions.

We also find that, if the TGCs can be measured with much better precisions, such as the ones in Ref. [4] for ILC 250 GeV (which are one order of magnitude better than the ones in Table 3), or if multiple runs with different beam polarizations are available (also likely to

1) It is reasonable to fix the background (which has no Higgs) to the SM predictions in an EFT global framework in this case, as deviations from SM are strongly constrained by the electroweak precision measurements at Z-pole or other measurements. Fixing the background nevertheless requires one to have a very good knowledge of the total rate and distribution shape of the background, as pointed out in Section 2.

be the case for ILC), the improvement from the $m_{\rm recoil}$ and $m^p_{\rm recoil}$ distributions with respect to using only the total rate of $e^+e^- \to \nu\bar{\nu}h$ becomes rather insignificant. This is not surprising, since very precise TGC measurements can effectively remove two degrees of freedom in the fit so that there is less need for additional handles to discriminate the parameters. The interference term of the $e^+e^- \to hZ$ diagram with an s-channel Z and the one with an s-channel photon are also sensitive to the beam polarization, which can help probe the operators that contribute to this interference [3, 4]. In general, once a sufficient number of constraints are included in a global analysis, the overall precision reach is expected to be less sensitive to the impact of a single measurement, such as that of $e^+e^- \to \nu\bar{\nu}h$. It is nevertheless important to optimize the measurements in order to maximize the sensitivity to new physics.

4 Applications to inclusive hZ measurements

While we have focused on the WW-fusion measurements in the previous two sections, a question of great interest is whether the variable $m^p_{\rm recoil}$ could be applied to improve the inclusive measurement of $e^+e^- \to hZ$, where the decay product of Z are tagged instead. While suffering from the jet resolution, the hadronic Z decay channel provides a slightly better measurement of $\sigma(Zh)$ than the leptonic one, thanks to its large branching ratio[1)]. An improved measurement of the hadronic Z channel could thus have a significant impact on the overall precision reach of $\sigma(hZ)$. It is straightforward to write down the recoil mass and its two variations for the reconstruction of the Higgs mass in $e^+e^- \to hZ$, which are

$$\begin{aligned} m^2_{\rm recoil} &= s-2\sqrt{s}E^{\rm rec}_Z+(m^{\rm rec}_Z)^2, \\ (m^E_{\rm recoil})^2 &= s-2\sqrt{s}E^{\rm rec}_Z+m^2_Z, \\ (m^p_{\rm recoil})^2 &= s-2\sqrt{s}\sqrt{m^2_Z+|\vec{p}^{\rm rec}_Z|^2}+m^2_Z, \end{aligned} \tag{12}$$

where $E^{\rm rec}_Z$, $\vec{p}^{\rm rec}_Z$ and $m^{\rm rec}_Z$ are the reconstructed energy, 3-momentum and invariant mass of the Z from the two jets, while m_Z is the true Z mass, fixed to be 91.19 GeV. Similar to Eq. (9), we derive the deviations in the measured $m_{\rm recoil}$, $m^E_{\rm recoil}$, $m^p_{\rm recoil}$ as a function of the deviations in the measured Z energy and 3-momentum to be

$$\delta_m \ / \ \delta^E_m \ / \ \delta^p_m \approx \begin{cases} -0.91\delta_E-0.17\delta_p \ / \ -1.6\delta_E \ / \ -0.39\delta_p & \text{at 240GeV} \\ -0.99\delta_E-0.25\delta_p \ / \ -1.8\delta_E \ / \ -0.56\delta_p & \text{at 250GeV} \end{cases}, \tag{13}$$

where δ_m, δ^E_m and δ^p_m are defined as

$$m_{\rm recoil}= m^{\rm true}_{\rm recoil}(1+\delta_m), \quad m^E_{\rm recoil}=m^{\rm true}_{\rm recoil}(1+\delta^E_m), \quad m^p_{\rm recoil}=m^{\rm true}_{\rm recoil}(1+\delta^p_m), \tag{14}$$

with $m^{\rm true}_{\rm recoil}=m_h$. For δ_E and δ_p, the definitions are

$$E^{\rm rec}_Z= E_Z(1+\delta_E), \qquad |\vec{p}^{\rm rec}_Z|=|\vec{p}_Z|(1+\delta_p), \tag{15}$$

where E_Z and $\vec{p}_Z$ are the true energy and 3-momentum of the Z. Similar to Eq. (9), in Eq. (13) the coefficients of δ_p are also smaller than those of δ_E, but with a suppression factor of $\sim|\vec{p}_Z|^2/E^2_Z$ instead. The distributions of δ_E and δ_p for the reconstructed Z are shown in Fig. 6, with the details of simulation stated later in this section. Note that the cut on the Z-mass window has a strong impact on the distributions of δ_E and δ_p. For larger deviations of the measured energy and momentum from the true ones, the invariant mass also tends to be further away from its true value.

To compare the reconstruction power of $m_{\rm recoil}$ and $m^p_{\rm recoil}$ on the Higgs mass, we perform a simple analysis using the simulation tools listed in Section 2. One important difference here is that for Higgs inclusive measurement with $Z\to q\bar{q}$, the final states could contain additional jets from Higgs decay, making it more difficult to reconstruct the Z. Due to the additional jets, we set the jet radius to R=0.5 in order to reduce the contamination among the jets. For an event with more than two jets, we choose the pair of jets with an invariant mass that is closest to the value of Z mass. We then apply a Z-mass-window cut on the invariant mass of the jet pair, $m_{q\bar{q}}$, intended for removing backgrounds. The difference between $m_{\rm recoil}$ and $m^p_{\rm recoil}$ is strongly correlated with the size of the Z window – in the limit that the invariant mass equals the actual Z mass, $m_{\rm recoil}$ and $m^p_{\rm recoil}$ become equivalent. We therefore consider both a larger window, $70{\rm GeV} < m_{q\bar{q}} < 110{\rm GeV}$, and a smaller one, $80{\rm GeV} < m_{q\bar{q}} < 95{\rm GeV}$. The distributions of $m_{\rm recoil}$ and $m^p_{\rm recoil}$ for $e^+e^- \to hZ, Z\to q\bar{q}$ after the selection cuts are shown in Fig. 7 for CEPC 240 GeV. To estimate the impact of the combinatorial problem in the reconstruction of Z, we first consider a case in which the Higgs is forced to decay invisibly in the simulation. The only purpose of the invisible decay is to avoid having additional jets from the Higgs decay and ensure a clear identification of the Z jet-pair. The results are shown in the top panels of Fig. 7 for the two choices of Z-mass-window cuts.

1) For instance, the precision of the inclusive hZ cross section measured from the leptonic (hadronic) Z channel is reported to be 0.8% (0.65%) in the CEPC preCDR [6].

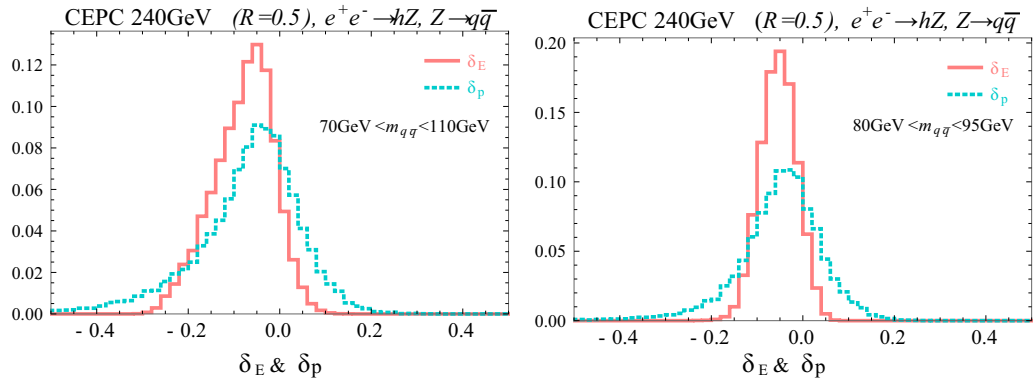

Fig. 6. (color online) The distributions of δ_E and δ_p of the reconstructed Z (defined in Eq. (15)) in $e^+e^- \to hZ, Z \to q\bar{q}$ at CEPC 240 GeV after applying a Z-mass-window cut of $70\text{GeV} < m_{q\bar{q}} < 110\text{GeV}$ (a) or $80\text{GeV} < m_{q\bar{q}} < 95\text{GeV}$ (b). The Higgs is forced to decay invisibly in the simulation to ensure the correct reconstruction of Z. A radius of R=0.5 is used in the jet clustering algorithm.

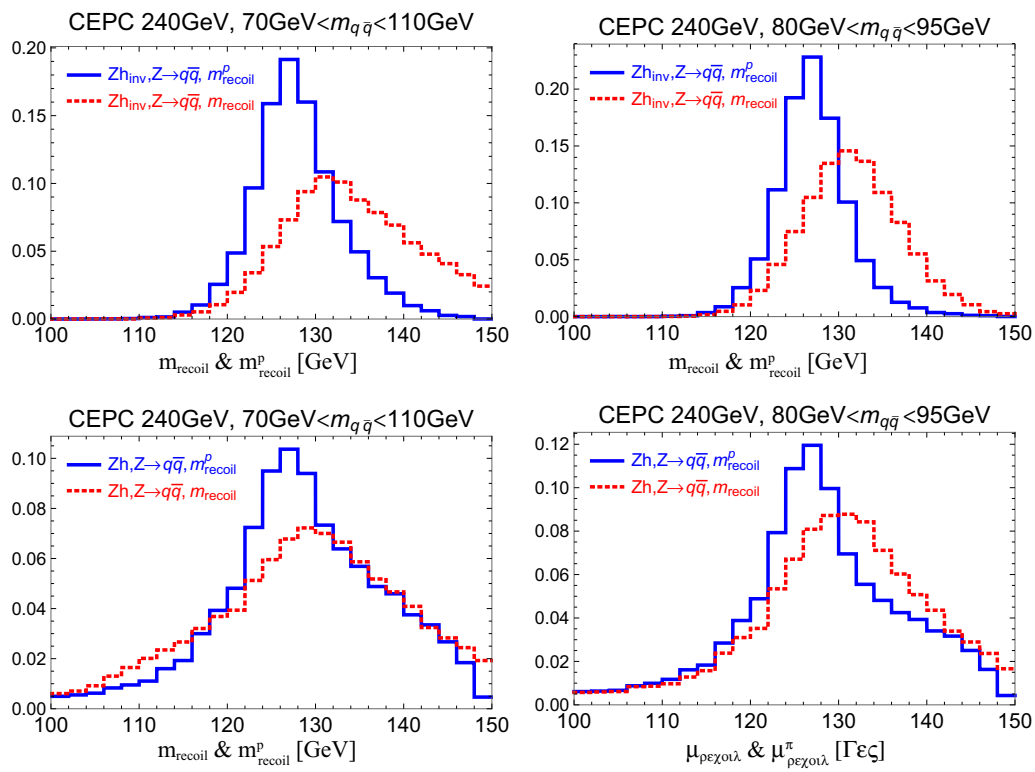

Fig. 7. (color online) Top row: The distributions of m_{recoil} and m^p_{recoil} for $e^+e^- \to hZ, Z \to q\bar{q}$ at CEPC 240 GeV. The Higgs is forced to decay invisibly in the simulation to avoid the combinatorial problem. Bottom row: The same distributions with Higgs inclusive decay. The left and right panels differ on the Z-mass-window cut, which is $70\text{GeV} < m_{q\bar{q}} < 110\text{GeV}$ ($80\text{GeV} < m_{q\bar{q}} < 95\text{GeV}$) for the left (right) panels.

For this ideal case, it is clearly that m^p_{recoil} has a significantly narrower spread and provides a much better reconstruction of the Higgs mass than m_{recoil} does. The improvement with m^p_{recoil} is more significant if a large Z-mass window cut is applied as we expected. For the realistic case with Higgs inclusive decays, the distributions are shown in the bottom panels of Fig. 7. The reconstruction of the Higgs mass is worse for both m_{recoil} and m^p_{recoil} distributions due to the wrong jet-pairing. However, m^p_{recoil} still has a better performance than m_{recoil}, so its usefulness is not washed out by the combinatorial problem. We also note that, due to the lack of jet energy

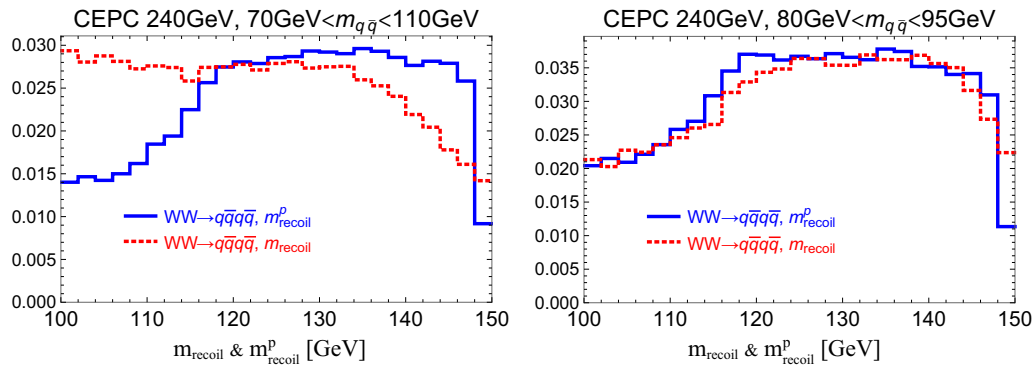

Fig. 8. (color online) The distributions of $m_{\rm recoil}$ and $m^p_{\rm recoil}$ for $W^+W^-\to q\bar{q}q\bar{q}$ at CEPC 240 GeV with a Z-mass-window cut of 70GeV$<m_{q\bar{q}}<$110GeV (a) or 80GeV$<m_{q\bar{q}}<$95GeV (b).

correction mentioned in Section 2, our distributions of $m_{\rm recoil}$ peak around 130 GeV rather than 125 GeV. While the central values of the distributions can be corrected, we expect $m^p_{\rm recoil}$ to still have a better performance than $m_{\rm recoil}$ after the implementation of jet energy corrections due to the parametric suppression on the uncertainties of $m^p_{\rm recoil}$ near the hZ threshold.

Since the background events do not have Higgs in them, we do not expect their $m^p_{\rm recoil}$ distributions to accumulate around the Higgs mass. As a simple estimation, we show the $m_{\rm recoil}$ and $m^p_{\rm recoil}$ distributions for one of the main backgrounds, $W^+W^-\to q\bar{q}q\bar{q}$ in Fig. 8, also for both choices of the Z-mass-window cuts. It is interesting to notice that for the larger Z mass window, $m^p_{\rm recoil}$ actually reduces the number of background events in the region of ∼100–120 GeV, while for the smaller window, the $m_{\rm recoil}$ and $m^p_{\rm recoil}$ distributions are very similar.

Our study shows that the $m^p_{\rm recoil}$ variable could reconstruct the Higgs mass better for the signal and does not have the same effect on backgrounds. As such, we expect it to provide a significant improvement on the inclusive cross section measurements of the Higgsstrahlung process compared with the conventional recoil mass variable $m_{\rm recoil}$. Needless to say, such an improvement is crucially relevant to studies of the Higgs boson properties. We also find similar behavior for the signal and background distributions at the ILC 250 GeV, the results of which are not specifically shown. Since we have only performed a simplified simulation analysis and have not considered some of the important backgrounds, we will restrain ourselves from doing any quantitative analysis on the inclusive $\sigma(hZ)$ measurements and leave it for experimental groups who have better tools for such an analysis.

5 Conclusions

In this paper, we have explored the use of the recoil mass and its variations in the measurements of the WW-fusion process at a lepton collider with a center of mass energy of 240–250 GeV. We found the variable $m^p_{\rm recoil}$, constructed using only the 3-momenta of the Higgs decay products, can separate Higgsstrahlung events with an invisible Z from the WW-fusion events better than the original recoil mass $m_{\rm recoil}$ does, with an improvement up to 20%–30% on the precision of the WW-fusion cross section. We have studed its impact in both the conventional framework and the effective-field-theory one. In the conventional framework, a better precision on the WW-fusion cross section leads to a significant improvement on the constraints of the hWW coupling and the total Higgs width. In a global analysis under the effective-field-theory framework, using the information in the $m_{\rm recoil}$ or $m^p_{\rm recoil}$ distributions could improve the reach on some of the EFT parameters by more than 10% compared with just using the total rate of the $e^+e^-\to\nu\bar{\nu}h$ channel. We find that fitting the EFT parameters directly to the binned distributions gives the best precision reach. On the other hand, if the EFT parameters are fitted to the precisions of the WW-fusion and $hZ, Z\to\nu\bar{\nu}$ cross sections extracted from the $m_{\rm recoil}$ distribution, the precision reach could suffer from the large correlation between the two cross sections if it is not taken account of. We have also explored the use of $m^p_{\rm recoil}$ in the inclusive measurements of the Higgsstrahlung process ($e^+e^-\to hZ$) with hadronic Zs and find that it can significantly improve the reconstruction of the Higgs at a center of mass energy of 240–250 GeV. The use of $m^p_{\rm recoil}$ could therefore potentially lead to an improvement in the overall precision of the inclusive hZ cross section measurements.

The construction of $m^p_{\rm recoil}$ is extremely simple and does not require any additional measurements. In fact, $m^p_{\rm recoil}$ is a one-to-one function of $|\vec{p}^{\rm rec}|$, the magnitude of the reconstructed 3-momentum of the visible particle. In terms of the discrimination between signal and backgrounds, $|\vec{p}^{\rm rec}|$ and $m^p_{\rm recoil}$ are in principle equivalent. In the future, conventional analyses using the recoil mass variables may also be replaced by multivariable analyses which can extract the maximum amount of informa-

tion from the measured quantities. Nevertheless, the construction of $m^p_{\rm recoil}$ still provides important physical understanding in terms of its better performance in the mass reconstruction. It should be straightforward to implement $m^p_{\rm recoil}$ in studies that make use of the recoil mass distribution.

We thank Tao Liu, Zhen Liu, Junping Tian and Yan Wang for useful discussions and valuable comments on the manuscript.

Appendix A

"12 (or 11)-parameter" effective-field-theory framework

We follow the framework in Ref. [3], which uses the Higgs basis, proposed in Ref. [33] and applied also in the studies of LHC Higgs measurements in Refs. [30, 34]. We focus on CP-even dimension-6 (D6) operators and omit the ones that induce fermion dipole interactions. We also assume the Z-pole observables and W mass to be SM-like, given that they are already very well constrained by LEP and can be further constrained with a Z-pole run at the future lepton colliders.

The relevant parts in the Lagrangian of the SM and D6 operators are

$$\mathcal{L}\supset\mathcal{L}_{hVV}+\mathcal{L}_{hff}+\mathcal{L}_{\rm tgc}, \tag{A1}$$

where the Higgs boson couplings to a pair of SM gauge bosons are given by

$$\begin{aligned}\mathcal{L}_{hVV}=\frac{h}{v}\Big[&(1+\delta c_W)\frac{g^2v^2}{2}W^+_\mu W^{-\mu}\\&+(1+\delta c_Z)\frac{(g^2+g'^2)v^2}{4}Z_\mu Z^\mu\\&+c_{WW}\frac{g^2}{2}W^+_{\mu\nu}W^{-\mu\nu}+c_{W\Box}g^2(W^-_\mu\partial_\nu W^{+\mu\nu}+\text{h.c.})\\&+c_{gg}\frac{g_s^2}{4}G^a_{\mu\nu}G^{a\mu\nu}+c_{\gamma\gamma}\frac{e^2}{4}A_{\mu\nu}A^{\mu\nu}\\&+c_{Z\gamma}\frac{e\sqrt{g^2+g'^2}}{2}Z_{\mu\nu}A^{\mu\nu}+c_{ZZ}\frac{g^2+g'^2}{4}Z_{\mu\nu}Z^{\mu\nu}\\&+c_{Z\Box}g^2Z_\mu\partial_\nu Z^{\mu\nu}+c_{\gamma\Box}gg'Z_\mu\partial_\nu A^{\mu\nu}\Big].\end{aligned} \tag{A2}$$

The parameters in Eq. (A2) are not all independent. Four constraints can be written down by imposing gauge invariances, for which we choose to rewrite δc_W, c_{WW}, $c_{W\Box}$ and $c_{\gamma\Box}$ as

$$\begin{aligned}\delta c_W&=\delta c_Z+4\delta m,\\c_{WW}&=c_{ZZ}+2s^2_{\theta_W}c_{Z\gamma}+s^4_{\theta_W}c_{\gamma\gamma},\\c_{W\Box}&=\frac{1}{g^2-g'^2}\big[g^2c_{Z\Box}+g'^2c_{ZZ}-e^2s^2_{\theta_W}c_{\gamma\gamma}\\&\qquad-(g^2-g'^2)s^2_{\theta_W}c_{Z\gamma}\big],\\c_{\gamma\Box}&=\frac{1}{g^2-g'^2}\big[2g^2c_{Z\Box}+(g^2+g'^2)c_{ZZ}-e^2c_{\gamma\gamma}\\&\qquad-(g^2-g'^2)c_{Z\gamma}\big],\end{aligned} \tag{A3}$$

where δm can only be induced by custodial symmetry breaking effects and is set to zero in our framework. For the Yukawa couplings, we focus on those of t, c, b, τ, μ, parameterized as

$$\mathcal{L}_{hff}=-\frac{h}{v}\sum_{\rm f=t,c,b,\tau,\mu}m_f(1+\delta y_f)\bar{f}_Rf_L+\text{h.c.}. \tag{A4}$$

Possible flavor-violating Yukawa couplings from new physics are not considered. The anomalous triple gauge couplings (aTGCs) are parameterized as

$$\begin{aligned}\mathcal{L}_{\rm tgc}=\;&igs_{\theta_W}A^\mu(W^{-\nu}W^+_{\mu\nu}-W^{+\nu}W^-_{\mu\nu})\\&+ig(1+\delta g^Z_1)c_{\theta_W}Z^\mu(W^{-\nu}W^+_{\mu\nu}-W^{+\nu}W^-_{\mu\nu})\\&+ig[(1+\delta\kappa_Z)c_{\theta_W}Z^{\mu\nu}+(1+\delta\kappa_\gamma)s_{\theta_W}A^{\mu\nu}]W^-_\mu W^+_\nu\\&+\frac{ig}{m^2_W}(\lambda_Zc_{\theta_W}Z^{\mu\nu}+\lambda_\gamma s_{\theta_W}A^{\mu\nu})W^{-\rho}_vW^+_{\rho\mu},\end{aligned} \tag{A5}$$

where $V_{\mu\nu}\equiv\partial_\mu V_\nu-\partial_\nu V_\mu$ for $V=W^\pm,Z,A$. Gauge invariance further imposes the relations $\delta\kappa_Z=\delta g_{1,Z}-t^2_{\theta_W}\delta\kappa_\gamma$ and $\lambda_Z=\lambda_\gamma$. This leaves three independent aTGC parameters, which we choose to be $\delta g_{1,Z}$, $\delta\kappa_\gamma$ and λ_Z. Two of them, $\delta g_{1,Z}$ and $\delta\kappa_\gamma$, are related to the Higgs parameters and can be written as

$$\begin{aligned}\delta g_{1,Z}=\;&\frac{1}{2(g^2-g'^2)}\big[-g^2(g^2+g'^2)c_{Z\Box}-g'^2(g^2+g'^2)c_{ZZ}\\&+e^2g'^2c_{\gamma\gamma}+g'^2(g^2-g'^2)c_{Z\gamma}\big],\\\delta\kappa_\gamma=\;&-\frac{g^2}{2}\left(c_{\gamma\gamma}\frac{e^2}{g^2+g'^2}+c_{Z\gamma}\frac{g^2-g'^2}{g^2+g'^2}-c_{ZZ}\right).\end{aligned} \tag{A6}$$

To summarize, in our framework the contribution from D6 operators to the Lagrangian in Eq. (A1) can be parametrized by the following 12 parameters:

$$\begin{aligned}&\delta c_Z,\;\; c_{ZZ},\;\; c_{Z\Box},\;\; c_{\gamma\gamma},\;\; c_{Z\gamma},\;\; c_{gg},\\&\delta y_t,\;\; \delta y_c,\;\; \delta y_b,\;\; \delta y_\tau,\;\; \delta y_\mu,\;\; \lambda_Z.\end{aligned} \tag{A7}$$

Also following Refs. [3, 30, 34], we consider the EFT contribution to the hγγ and hZγ vertices at the tree level, in which case the only EFT parameter that contributes to the decay rate of h→γγ (h→Zγ) is $c_{\gamma\gamma}$ ($c_{Z\gamma}$). For the decay h→gg, we include, in addition to c_{gg}, the contributions of δy_t and δy_b, which enter the hgg vertex by modifying the Yukawa couplings in the fermion loops. It is also convenient to normalize $c_{\gamma\gamma}$, $c_{Z\gamma}$ and c_{gg} with respect to the SM 1-loop contributions. We follow Ref. [3] and define the following parameters

$$\frac{\Gamma_{\gamma\gamma}}{\Gamma^{\rm SM}_{\gamma\gamma}}\simeq1-2\bar{c}_{\gamma\gamma},\qquad\frac{\Gamma_{Z\gamma}}{\Gamma^{\rm SM}_{Z\gamma}}\simeq1-2\bar{c}_{Z\gamma}, \tag{A8}$$

and

$$\frac{\Gamma_{gg}}{\Gamma_{gg}^{\rm SM}} \simeq 1+2\bar{c}_{gg}^{\rm eff} \simeq 1+2\bar{c}_{gg}+2.10\delta y_t-0.10\delta y_b, \qquad (A9)$$

where $\bar{c}_{\gamma\gamma}$, $\bar{c}_{Z\gamma}$ and $\bar{c}_{gg}$ are related to the original parameters by

$$\bar{c}_{\gamma\gamma}\simeq\frac{c_{\gamma\gamma}}{8.3\times10^{-2}},\ \ \bar{c}_{Z\gamma}\simeq\frac{c_{Z\gamma}}{5.9\times10^{-2}},\ \ \bar{c}_{gg}\simeq\frac{c_{gg}}{8.3\times10^{-3}}. \qquad (A10)$$

Furthermore, without measuring the $t\bar{t}h$ process at high energies ($\sqrt{s}\gtrsim$500GeV) or at the LHC, the parameters c_{gg} and δy_t cannot be independently constrained. Since we focus on the 240-250 GeV run at lepton colliders, we replace c_{gg} and δy_t by $\bar{c}_{gg}^{\rm eff}$ in Eq. (A9) which parametrize the total contribution to the hgg vertex. The number of parameters is thus reduced to 11, and the parameters are

$$\delta c_Z,\ \ c_{ZZ},\ \ c_{Z\Box},\ \ \bar{c}_{\gamma\gamma},\ \ \bar{c}_{Z\gamma},$$
$$\bar{c}_{gg}^{\rm eff},\ \ \delta y_c,\ \ \delta y_b,\ \ \delta y_\tau,\ \ \delta y_\mu,\ \ \lambda_Z, \qquad (A11)$$

which are used in our EFT global analysis in Section 3.

Appendix B

EFT expressions for $e^+e^-\to\nu\bar{\nu}h$ cross sections

We obtain the cross section of $e^+e^-\to\nu\bar{\nu}h$ as a function of the EFT parameters by generating events using `Madgraph5` [15] with the `BSMC` package [35, 36]. The events are showered in `Pythia` [16] and passed to `Delphes` [17] with the ILD card for detector simulations, after which the selection cuts in Section 2 are applied. The interference between hZ and WW fusion is also included. The results for CEPC 240 GeV with unpolarized beams are listed as follows. For the total rate, we have

$$\left.\frac{\sigma_{\nu\bar{\nu}h}}{\sigma_{\nu\bar{\nu}h}^{\rm SM}}\right|_{240{\rm GeV}}^{\rm unpolarized} = 1+1.7\delta c_Z+1.3c_{ZZ}+2.9c_{Z\Box} +0.051c_{Z\gamma}+0.14c_{\gamma\Box} +0.23\delta c_W-0.0026c_{WW}-0.065c_{W\Box}. \qquad (B1)$$

Here we do not impose the gauge invariance condition from Eq. (A3), in order to show the different dependences on the Z and W parameters. For the binned differential distributions of $m_{\rm recoil}$ ($m_{\rm recoil}^p$), the numerical coefficients in Eq. (B1) are replaced by the ones in Table A1 (Table A2).

We have also checked that the statistical uncertainties from simulation are under control[1)]. We then impose the gauge invariance condition in Eq. (A3) and construct χ^2 of the $e^+e^-\to\nu\bar{\nu}h$ measurement, assuming the events follow a Poisson distribution. For the total rate, we have

$$\chi^2=\frac{N_{\rm sig}^2\left(1-\frac{\sigma_{\nu\bar{\nu}h}}{\sigma_{\nu\bar{\nu}h}^{\rm SM}}\right)^2}{N_{\rm sig}+N_{\rm bg}}, \qquad (B2)$$

where $N_{\rm sig}$ and $N_{\rm bg}$ are the number of signal and backgrounds after cuts, normalized to $5{\rm ab}^{-1}$ for CEPC. For the binned distributions, we use Eq. (B2) to construct the χ^2 of each bin, where $N_{\rm sig}$ and $N_{\rm bg}$ are the number of signal and backgrounds in the bin. We then sum over the χ^2 of all the bins, assuming no correlation among them. The χ^2 is then combined with those of other measurements for the global analysis in Section 3. We refer the readers to Ref. [3] for a complete set of expressions for the other relevant observables.

Table A1. The coefficients of the EFT parameters for the expression of $\sigma/\sigma_{\rm SM}$ of each bin of the $m_{\rm recoil}$ distribution. The upper bound of each bin is listed in the first row. The first bin include all the events below 75 GeV.

	CEPC 240 GeV (with unpolarized beams) $m_{\rm recoil}$									
	bin index/GeV									
	75	80	85	90	95	100	105	110	115	130
σ_{SM}/fb	0.15	0.18	0.38	0.78	1.2	1.3	1.1	0.74	0.47	0.34
δc_Z	0.97	1.4	1.6	1.7	1.8	1.9	1.9	1.9	1.8	1.9
c_{ZZ}	0.50	0.95	1.1	1.3	1.3	1.4	1.4	1.4	1.4	1.4
$c_{Z\Box}$	1.5	2.2	2.6	2.9	3.0	3.0	3.2	3.1	3.1	3.0
$c_{Z\gamma}$	0.021	0.035	0.044	0.051	0.052	0.054	0.056	0.056	0.055	0.055
$c_{\gamma\Box}$	0.075	0.11	0.13	0.14	0.15	0.15	0.15	0.15	0.15	0.15
δc_W	0.93	0.62	0.37	0.22	0.15	0.13	0.14	0.17	0.20	0.29
c_{WW}	−0.011	−0.0066	−0.0038	−0.0023	−0.0016	−0.0013	−0.0013	−0.0016	−0.0019	−0.0023
$c_{W\Box}$	−0.30	−0.18	−0.11	−0.060	−0.038	−0.032	−0.033	−0.036	−0.037	−0.049

1) There are nevertheless some small fluctuations in our result. For instance, the coefficients of δc_Z and δc_W should always add up to two. In most bins, the sum is controlled in the range 1.9–2.1. After imposing $\delta c_Z=\delta c_W$ we simply fix its coefficient to 2. We do not expect the fluctuations in other coefficients to significantly change our results.

Table A2. The coefficients of the EFT parameters for the expression of $\sigma/\sigma_{\rm SM}$ of each bin of the $m^p_{\rm recoil}$ distribution. The upper bound of each bin is listed in the first row. The first bin include all the events below 75 GeV.

	CEPC 240 GeV (with unpolarized beams) $m^p_{\rm recoil}$							
	bin index/GeV							
	75	80	85	90	95	100	105	115
σ_{SM}[fb]	0.22	0.24	0.59	1.7	2.4	0.99	0.32	0.11
δc_Z	0.95	1.4	1.7	1.8	1.9	2.0	1.8	1.4
c_{ZZ}	0.54	0.99	1.2	1.3	1.4	1.4	1.4	1.0
$c_{Z\Box}$	1.6	2.3	2.6	3.0	3.2	3.3	3.1	2.0
$c_{Z\gamma}$	0.021	0.035	0.045	0.053	0.056	0.059	0.054	0.044
$c_{\gamma\Box}$	0.075	0.11	0.13	0.15	0.16	0.16	0.15	0.11
δc_W	0.92	0.61	0.33	0.14	0.075	0.11	0.33	0.99
c_{WW}	−0.0095	−0.0062	−0.0034	−0.0014	−0.00082	−0.0012	−0.0025	−0.0075
$c_{W\Box}$	−0.28	−0.17	−0.092	−0.037	−0.019	−0.025	−0.056	−0.13

References

1 R. Lafaye, T. Plehn, M. Rauch, and D. Zerwas, *Higgs Factories: Higgs-Strahlung versus W-Fusion*, arXiv:1706.02174

2 J. Ellis and T. You, JHEP, **03**: 089 (2016), arXiv:1510.04561

3 G. Durieux, C. Grojean, J. Gu, and K. Wang, JHEP, **09**: 014 (2017), arXiv:1704.02333

4 T. Barklow, K. Fujii, S. Jung, R. Karl, J. List, T. Ogawa, M. E. Peskin, and J. Tian, *Improved Formalism for Precision Higgs Coupling Fits*, arXiv:1708.08912

5 W. H. Chiu, S. C. Leung, T. Liu, K.-F. Lyu, and L.-T. Wang, *Probing 6D Operators at Future e^-e^+ Colliders*, arXiv:1711.04046

6 CEPC-SPPC Study Group, CEPC-SPPC Preliminary Conceptual Design Report.1. Physics and Detector (2015)

7 A. Blondel, "Summary FCC-ee experiments." https://indico.cern.ch/event/556692/contributions/2487579/attachments/1469993/2274251/99-Blondel-FCC-ee-summary-Berlin.eps, 2017

8 H. Baer, T. Barklow, K. Fujii, Y. Gao, A. Hoang, S. Kanemura, J. List, H. E. Logan, A. Nomerotski, M. Perelstein et al, *The International Linear Collider Technical Design Report - Volume 2: Physics*, arXiv:1306.6352

9 D. M. Asner et al., *ILC Higgs White Paper*, in Proceedings, Community Summer Study 2013: Snowmass on the Mississippi (CSS2013): Minneapolis, MN, USA, July 29-August 6, 2013, 2013 arXiv:1310.0763

10 C. Dürig, K. Fujii, J. List, and J. Tian, *Model Independent Determination of HWW coupling and Higgs total width at ILC*, in International Workshop on Future Linear Colliders (LCWS13) Tokyo, Japan, November 11-15, 2013, 2014 arXiv:1403.7734

11 T. Barklow, J. Brau, K. Fujii, J. Gao, J. List, N. Walker, and K. Yokoya, *ILC Operating Scenarios*, arXiv:1506.07830

12 TLEP Design Study Working Group Collaboration, M. Bicer et al, JHEP, **01**: 164 (2014), arXiv:1308.6176

13 CMS Collaboration, V. Khachatryan et al., JINST,**12**(02): P02014 (2017), arXiv:1607.03663

14 ATLAS Collaboration, M. Aaboud et al, *Jet energy scale measurements and their systematic uncertainties in proton-proton collisions at $\sqrt{s} = 13$ TeV with the ATLAS detector*, arXiv:1703.09665

15 J. Alwall, R. Frederix, S. Frixione, V. Hirschi, F. Maltoni, O. Mattelaer, H. S. Shao, T. Stelzer, P. Torrielli, and M. Zaro, JHEP, **07**: 079 (2014), arXiv:1405.0301

16 T. Sjostrand, S. Mrenna, and P. Z. Skands, JHEP, **05**: 026 (2006), hep-ph/0603175

17 DELPHES 3 Collaboration, J. de Favereau, C. Delaere, P. Demin, A. Giammanco, V. Lemaître, A. Mertens, and M. Selvaggi, JHEP, **02**: 057 (2014), arXiv:1307.6346

18 H. Abramowicz et al, *The International Linear Collider Technical Design Report - Volume 4: Detectors*, arXiv:1306.6329

19 M. Greco, T. Han, and Z. Liu, Phys. Lett. B, **763**: 409–415 (2016), arXiv:1607.03210

20 J. Tian, "Update of e+e- −¿ nu nu h analysis at 250 GeV." https://agenda.linearcollider.org/event/7703/contributions/39487/attachments/31909/48179/vvh_20170719.eps, 2017

21 N. Craig, M. Farina, M. McCullough, and M. Perelstein, JHEP, **03**: 146 (2015), arXiv:1411.0676

22 M. Beneke, D. Boito, and Y.-M. Wang, JHEP, **11**: 028 (2014), arXiv:1406.1361

23 B. Henning, X. Lu, and H. Murayama, *What do precision Higgs measurements buy us*, arXiv:1404.1058

24 N. Craig, J. Gu, Z. Liu, and K. Wang, JHEP, **03**: 050 (2016), arXiv:1512.06877

25 J. Ellis, P. Roloff, V. Sanz, and T. You, JHEP, **05**: 096 (2017), arXiv:1701.04804

26 H. Khanpour and M. Mohammadi Najafabadi, Phys. Rev. D, **95**(5): 055026 (2017), arXiv:1702.00951

27 H. Denizli and A. Senol, *Constraints on Higgs effective couplings in $H\nu\bar{\nu}$ production of CLIC at 380 GeV* arXiv:1707.03890

28 T. Barklow, K. Fujii, S. Jung, M. E. Peskin, and J. Tian, *Model-Independent Determination of the Triple Higgs Coupling at e+e- Colliders*, arXiv:1708.09079

29 S. Di Vita, G. Durieux, C. Grojean, J. Gu, Z. Liu, G. Panico, M. Riembau, and T. Vantalon, *A global view on the Higgs self-coupling at lepton colliders*, arXiv:1711.03978

30 A. Falkowski, M. Gonzalez-Alonso, A. Greljo, and D. Marzocca, Phys. Rev. Lett., **116**(1): 011801 (2016), arXiv:1508.00581

31 M. Ruan, "Status & Updates from CEPC Simulation -Detector optimization." http://ias.ust.hk/program/shared_doc/2017/201701hep/HEP_20170124_Manqi_Ruan.eps, 2017

32 L. Bian, J. Shu, and Y. Zhang, JHEP, **09**: 206 (2015), arXiv:1507.02238

33 A. Falkowski, *Higgs Basis: Proposal for an EFT basis choice for LHC HXSWG*, LHCHXSWG-INT-2015-001 (March, 2015)

34 A. Falkowski, Pramana, **87**(3): 39 (2016), arXiv:1505.00046

35 B. Fuks and K. Mawatari, "The BSM Characterisation model." http://feynrules.irmp.ucl.ac.be/wiki/BSMCharacterisation, 2015

36 A. Falkowski, B. Fuks, K. Mawatari, K. Mimasu, F. Riva, and V. sanz, Eur. Phys. J. C, **75**(12): 583 (2015), arXiv:1508.05895